Solar flares detected by the new narrowband VLF receiver at SANAE IV

Authors:
Hanna Dahlgren[1,2]
Torbjörn Sundberg[1,3]
Andrew B. Collier[4,5]
Etienne Koen[1,4]
Stephen Meyer[4,5]

Affiliations:
[1]Space and Plasma Physics, Royal Institute of Technology, Stockholm, Sweden

[2]Department of Electrical and Computer Engineering and Center for Space Physics, Boston University, Boston, USA

[3]Heliophysics Science Division, NASA Goddard Space Flight Center, Greenbelt, USA

[4]SANSA Space Science, Hermanus, South Africa

[5]University of KwaZulu-Natal, Durban, South Africa

Correspondence to:
Hanna Dahlgren

Email:
hannad@bu.edu

Postal address:
725 Commonwealth Avenue, Room 408, Center for Space Physics, Boston 02215, Massachusetts, USA

A narrowband receiver was installed at the SANAE IV base in Antarctica to monitor specific very low frequency (VLF) radio signals from transmitters around the world. VLF waves propagating through the Earth–Ionosphere Waveguide are excellent probes of the varying properties of the lower region of the ionosphere. This paper describes the set-up of the narrowband system and demonstrates its capabilities with data from a set of solar flares on 08 February and 12 February 2010.

Introduction

Very low frequency (3 kHz – 30 kHz) radio waves propagate thousands of kilometres in the Earth-Ionosphere Waveguide (EIWG) formed between the conducting Earth and the ionosphere. During daytime, the ionospheric D-region (at an altitude of 60 km – 90 km) acts as the upper boundary of the EIWG, whilst at night the D-region becomes much weaker and the boundary moves to higher altitudes. Diurnal and seasonal changes in the ionosphere cause the reflection height of the EIWG to change in a predictable way,[1] whereas space weather events produce seemingly random modifications of the ionosphere, which affect the characteristics of the EIWG and therefore also VLF propagation.

High-power minimum shift keying (MSK) VLF transmitters operate at various locations around the world. The signals from these transmitters are extremely stable in both amplitude and phase. By monitoring them with narrowband VLF receivers, perturbations in the signal from a given transmitter can then be associated with ionospheric modification somewhere along the propagation path.

VLF radio signals can thus be used to probe the lower ionosphere. As this region is too high for atmospheric balloons and too low for satellites, it is one of the least studied regions of the Earth's atmosphere, and VLF waves are the only practical probes available. Estimates of D-region electron density have been determined via VLF propagation measurements.[2,3,4] Further information on the response of the D-region during ionospheric disturbances, such as solar flares and gamma ray bursts, can be retrieved by constantly monitoring single-frequency signals and their prompt response to changing conditions.

UltraMSK is a VLF narrowband receiver designed to measure both the amplitude and phase of modulated VLF signals. This paper describes the installation of UltraMSK on a VLF system at the SANAE IV base in Antarctica (72°40'S, 2°51'W). Data from several M-class and C-class solar flares illustrate the response of the instrument, and from these measurements the characteristics of the D-region can be modelled.

System set-up

UltraMSK was installed in parallel with the Digital VLF Recording and Analysis System[5] during February 2010. A magnetic loop antenna located a few hundred metres from SANAE IV was used for this purpose. The antenna consists of two vertically mounted diamond shaped loops with sides of length 7.6 m, aligned with the four cardinal directions. The loop facing north–south is a better choice for monitoring signals of European origin, whereas the east–west loop is more sensitive to signals propagating zonally.

Figure 1 shows a schematic of the UltraMSK system. A preamplifier at the base of the antenna boosts the signal, which is transmitted to the laboratory via a lengthy coaxial cable. The signal is passed through a second amplifier before reaching the service unit. From here the signal is transferred to the sound card on a personal computer. The service unit also integrates GPS timing. The phase of the signal is determined by a quadrature-phase mixer, where the received signal is split and mixed with an in-phase component on one hand and a quadrature-phase component on

the other. After the signals have been demodulated, the two components can be compared and information regarding the phase and amplitude of the signal can be extracted. In order to achieve a reliable centre frequency for the quadrature-phase mixer, the precise sampling frequency of the sound card is calibrated using the pulse-per-second signal from the GPS. The system runs at a sampling rate of 96 kHz, and the signal intensity and phase are recorded at 20 Hz.

In early 2009, the UltraMSK system was installed on a smaller (~1 m) omnidirectional whip antenna, but tests showed that this antenna did not provide an adequate signal-to-noise ratio (SNR), especially as it was positioned on top of the SANAE IV base, where disturbances from adjacent instruments and the base infrastructure were prominent. For this reason, the system was moved to the larger magnetic loop antenna. After testing and verification, the north–south loop was selected.

Identification of MSK frequencies

Very low frequency transmitter signals are expected to follow a regular diurnal pattern because of changes in the upper boundary of the EIWG resulting from the passage of the day–night terminator. The attenuation of the signal is higher during the day as a result of the lower conductivity of the D-region compared to the E-region at night. A typical quiescent diurnal pattern from the 18.3-kHz HWV transmitter in France is shown in Figure 2. The average daytime signal amplitude is about –65 dB, compared to –57 dB at night. Terminator effects can be seen during the dusk and dawn transitions, where changes in the D-region ionisation lead to dramatic changes in signal strength. The diurnal variation in power also leads to changes in the SNR. Because of this, the signal may be below the noise level during the day. This low level can be compensated for by applying a smoothing filter to the signal.

A number of VLF transmitter signals were identified at SANAE IV. Figure 3 shows a 5-min averaged spectrum for the north–south loop, where the MSK frequencies are marked by vertical dotted lines. Figure 4 illustrates the great circle paths between the corresponding transmitters and SANAE IV. An overview of transmitters is given in Table 1.[6] The 18.3-kHz HWV transmitter is currently the strongest signal in the spectrum. Several weaker signals of European origin are also present. Note, however, that these signals are subject to change, and the 16.4-kHz JXN transmitter in particular follows a discontinuous transmission pattern, generally transmitting for only a few hours daily.

In addition to the narrowband MSK signals in Figure 3, there is also a broader hump visible in the 4 kHz – 25 kHz range as a result of the radiation from lightning strokes. Lightning discharges around the world radiate most of their energy in the VLF band and thus constitute the main source of VLF waves propagating in the EIWG. When arriving at a receiver, they are seen as an impulsive broadband signal termed a 'sferic'. A network of VLF lightning location sensors, the World Wide Lightning Location Network (WWLLN) has
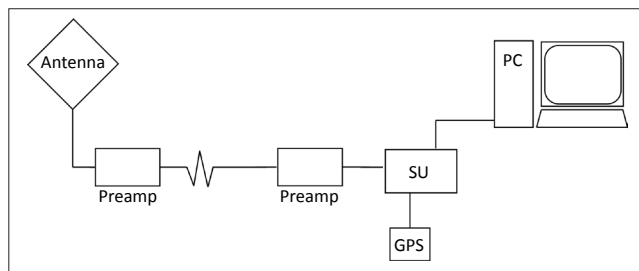
Preamp, preamplifier; SU, service unit; PC, personal computer; GPS, global positioning system.

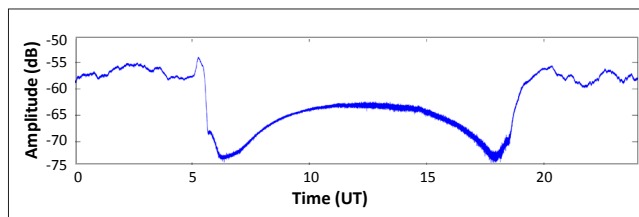**FIGURE 1:** Block diagram showing the structure of the UltraMSK system.

FIGURE 2: A typical diurnal power profile, measured at SANAE IV, for the 18.3-kHz HWV transmitter in France. Dips in the signal power as a result of the terminator effect can be seen at the dusk and dawn transitions (~06:00 and ~18:00).
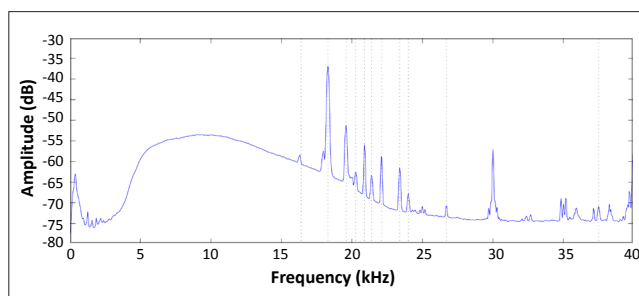

FIGURE 3: Averaged spectrum for 07 February 2010. The vertical dotted lines mark the frequencies of some known minimum shift keying transmitters. The broadband peak between 4 kHz and 25 kHz is as a result of sferics generated by global lightning activity.

been set up to map global lightning activity by combining the sferics detected at different locations around Earth.[7] SANAE IV also operates as a node in this network.

Several non-MSK peaks can also be seen in the spectrum, with the most prominent ones located at above 30 kHz and below 2 kHz. These disturbances likely originate from the electrical system at SANAE IV, and do not interfere with the monitored MSK signals.

In general, north–south paths are preferred as they allow a single local time to be studied. East–west paths are to a greater extent disturbed by dawn and dusk terminator effects. The main advantage of the east–west facing loop is the strong 1-MW 19.8-kHz NWC signal from Western Australia, although the signal strength is reduced as a result of extensive propagation over the Antarctic ice sheet. Because of SANAE IV's position relative to the global VLF transmitters, signals originating from the east or west travel a great distance over the Antarctic ice mass, as illustrated in Figure 4. The thickness of the ice layer can be a significant fraction of a wavelength, which implies increased attenuation as a result of the low
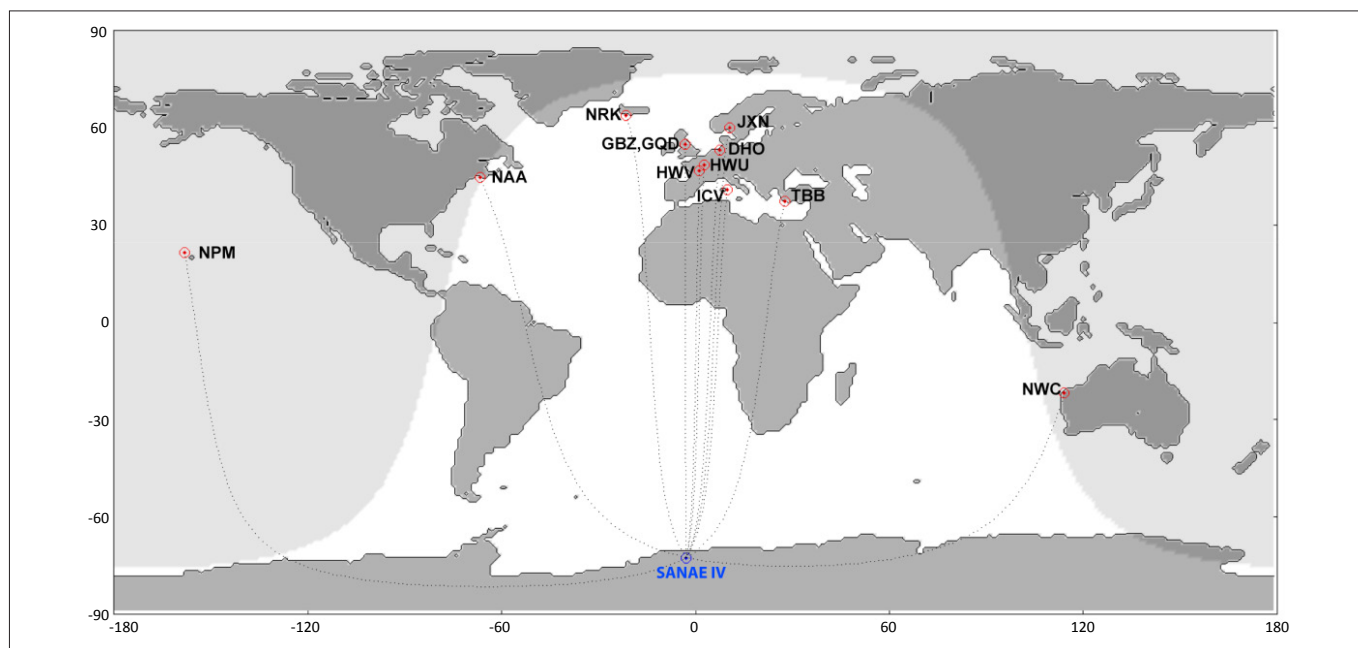
DHO, Germany; GBZ, England; GQD, England; HWU, France; HWV, France; ICV, Italy; JXN, Norway; NAA, Maine, USA; NPM, Hawaii; USA; NRK, Iceland; NWC, Australia; TBB, Turkey.

FIGURE 4: Great circle paths from various minimum shift keying transmitters to SANAE IV. The shading indicates the location of the day–night terminator at midday on 12 February 2010.

TABLE 1: Minimum shift keying frequencies identified at SANAE IV during February 2010.

Frequency (kHz)	Call name	Origin	Latitude	Longitude	GCP (Mm)	Estimated power (kW)
16.40	JXN	Norway	59°55′N	010°31′E	14.8	45
18.30	HWV	France	46°42′N	001°14′E	13.3	400
19.60	GBZ	England	54°53′N	003°17′W	14.2	100
19.80	NWC	Australia	21°49′N	114°10′W	8.7	1000
20.27	ICV	Italy	40°55′N	009°45′E	12.7	50
20.90	HWU	France	48°32′N	002°35′E	13.5	400
21.40	NPM	Hawaii, USA	21°26′N	158°09′W	14.1	500
22.10	GQD	England	54°53′N	003°17′W	14.2	60
23.40	DHO	Germany	53°05′N	007°37′E	14.0	300

Sources: Clilverd et al.[6] and Cohen MB 2010, personal communication, June 30
GCP, great circle paths.

conductivity of ice. This attenuation is typically 20 dB/Mm – 40 dB/Mm, whereas the attenuation over the sea is about 1 dB – 3 dB/Mm. Experimental data has shown even greater attenuation over ice (Barr[8] and references therein).[8]

Modelling the D-region

The ionospheric D-region is generally characterised by Wait's[9] parameters, H' and β, where H' (in km) is the reference height and β (in km^{-1}) the exponential sharpness factor. From these parameters, the electron density (N_e) as a function of altitude (z) can be described by[9,10]

$$N_e(z, H', \beta) = 1.43 \times 10^{13} \cdot e^{-0.15H'} \cdot e^{(\beta-0.15)(z-H')} \text{ [m}^{-3}\text{]}. \qquad \text{[Eqn 1]}$$

The Long-Wave Propagation Capability (LWPC) code was developed by the Naval Oceans Systems Center (San Diego, USA) to model the propagation of VLF signals. LWPC uses the electron density profile described by [Eqn 1] to model the ionosphere. A change in H' or β would lead to a modification in the EIWG, thus causing a change in the amplitude and phase of the signal. The modelled values of H' and β are modified iteratively to find a signal amplitude and phase

which matches the VLF measurements. The unperturbed values for H' and β depend on the solar zenith angle[10] and are derived from the empirical equations presented by McRae and Thomson[11]. In this study, estimates of H' and β were calculated using the average solar zenith angle along the north–south transmission path.

Event description and data analysis

Energy exchange between the magnetosphere and the surrounding solar wind is a continuous process which is enhanced during periods of increased solar activity. Coronal mass ejections and solar flares release an enormous number of highly energetically charged particles which are transported through the solar wind to Earth. These particles are accompanied by X-ray bursts, which are harmful to satellites, spacecraft and astronauts. These events have an appreciable impact on the Earth's ionosphere. The quiet-time ionospheric D-region is mainly maintained by Lyman-alpha radiation, with the flux of solar X-rays and gamma-rays being only a minor contributor. However, during solar flares there is a significant increase in radiation with a wavelength < 1 nm. This radiation penetrates down into the lower ionosphere

and leads to sudden ionospheric disturbances.[12] Solar flares cause a broad increase in plasma density in the dayside ionosphere, which in turn affects VLF signals propagating in the EIWG.

On 08 February 2010, several X-ray bursts associated with solar flares were detected by the Geostationary Operational Environmental Satellite (GOES) 14 satellite. The VLF signal from the 18.3-kHz HWV transmitter on 08 February 2010 is shown in Figure 5. As a comparison to illustrate a quiescent curve, the signal from 11 February 2010 is also shown. The corresponding GOES 14 X-ray (0.1 nm – 0.8 nm) flux data is plotted in the bottom panel of Figure 5. Four M-class flares (peak flux between 10^{-5} W/m^2 and 10^{-4} W/m^2) and a number of C-class flares (peak flux between 10^{-6} W/m^2 and 10^{-5} W/m^2) were detected during the day. The increases in X-ray flux are well correlated with the disturbances in the VLF signal. Two artificial spikes are present in Figure 5 at 07:50 and 11:38 (UTC), the first is as a result of a data dropout where the signal is temporarily lost during the solar flare event, and the second is a result of saturation in the received signal. These dropouts have no physical significance and can be disregarded in further analysis of the event.

Four days later, on 12 February 2010, two other M-class flares were detected in the GOES 14 data. The UltraMSK and GOES 14 data for this day are shown in Figure 6. The strongest flare had a flux of almost 10^{-4} W/m^2. As the second flare occurred around dusk, the associated VLF disturbance was superimposed onto terminator effects, which led to a general increase of the signal strength for the duration of the event.

Because of terminator effects, only events that took place close to midday (between 11:00 and 15:00) were analysed further. Two M-class flares and one C-class flare fulfilled this criterion in the 08 February data, shown in Figure 7. The times of the peaks of these flares were registered at 11:14, 12:03 and 13:47. The stronger M-class flare on 12 February had a peak flux at 11:26, as shown in Figure 7.

For all three M-class flares, the HWV signal strength experienced a rapid increase of 3 dB – 4 dB over a period of a few minutes, after which the intensity fell off again and returned to the unperturbed value about 30 min after the peak. For two of these events, the signal strength dipped after the peak, approximately 4 dB below the initial value, after which the amplitude slowly recovered during the next hour. The third flare also had a dip associated with it, but of smaller amplitude. This dip is believed to be a result of modal interference because the ionosphere gradually recovered to normal levels. Although the flux was significantly larger for the 12 February event, the increase in VLF signal strength was about the same as for the weaker M-class flare at 13:47 on 08 February.

Deviations in signal amplitude in nine of the monitored MSK signals for the 12 February 2010 event are shown in Figure 8. Because the event occurred near midday, the disturbance pattern was clearly visible in the signals of central European origin, at a similar longitude to SANAE IV. For these transmitters the signal increased in power by 4 dB – 6 dB. The main increase was more prominent in the stations located at other longitudes, that is, NPM on Hawaii, NAA in Maine and TBB in Turkey, with an increase of 8 dB – 14 dB.
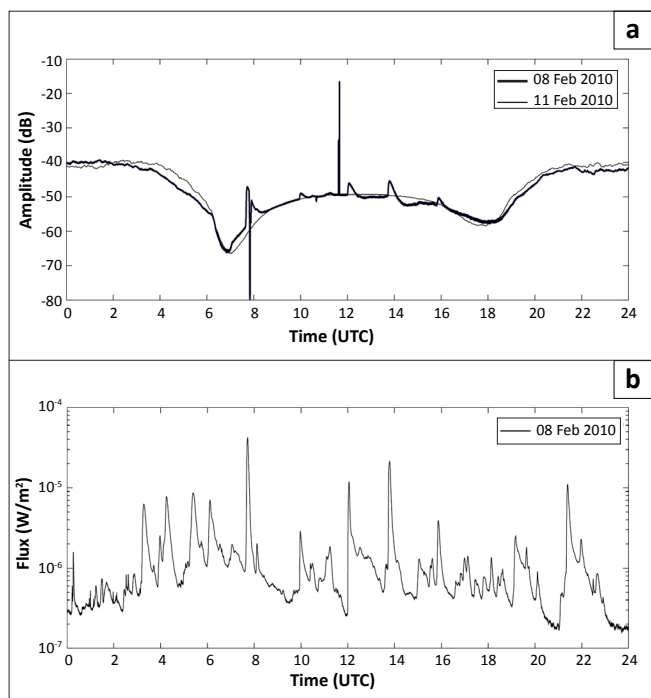
FIGURE 5: (a) Signal strength from the 18.3-kHz HWV transmitter in France on 08 February 2010 (thick line), showing fluctuations as a result of solar activity. The signal strength from a quiet day (11 February 2010, thin line) is plotted for comparison. (b) GOES 14 X-ray (0.1 nm – 0.8 nm) flux data from 08 February 2010, showing a number of C-class and M-class flares.
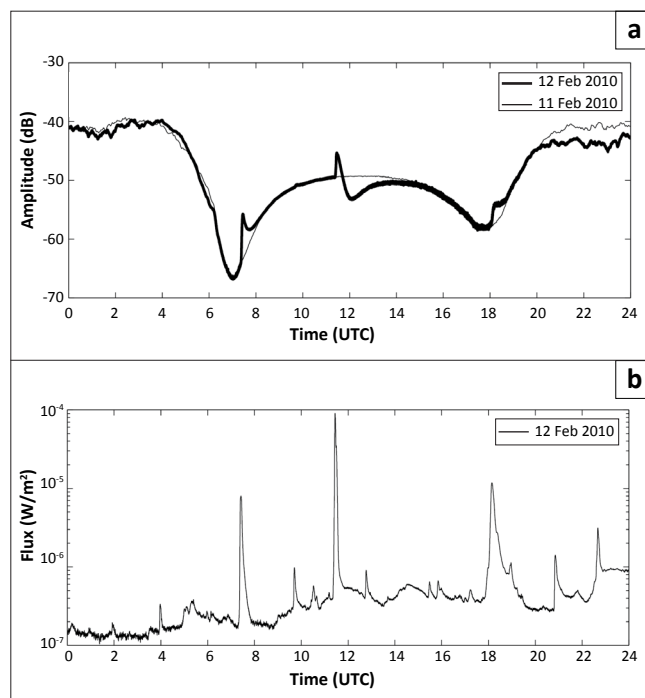
FIGURE 6: (a) Signal strength from the 18.3-kHz HWV transmitter in France on 12 February 2010 (thick line), showing fluctuations as a result of solar activity. The signal strength from a quiet day (11 February 2010, thin line) is plotted for comparison. (b) GOES 14 X-ray (0.1 nm – 0.8 nm) flux data from 12 February 2010, showing a number of C-class and M-class flares.
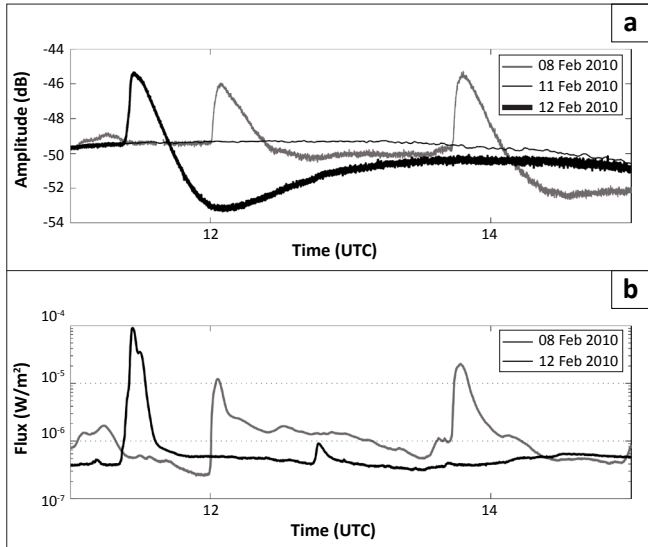
FIGURE 7: (a) X-ray flux (0.1 nm – 0.8 nm) for 11:00 – 15:00 on 08 February 2010 (thick grey line) and 12 February 2010 (thick black line) from the Geostationary Operational Environmental Satellite (GOES) 14. (b) 18.3-kHz HWV transmitter power from France for the same periods.

However, the subsequent decrease was partly drowned out as a result of the diurnal variations in the signals, so the power did not drop below the quiescent value after the flare.

Because of its stable phase during quiet conditions, the 23.4-kHz DHO signal was selected for the LWPC modelling of the H' and β parameters for the events. An instantaneous

increase in the phase was detected at the times of the flares, which then fell back to the quiescent state with a relaxation time in the order of 1 h. The unperturbed values for H' and β just before the 11:26 flare on 12 February were found to be 73.74 km and 0.334 km^{-1}, respectively. At the peak times of the flares, the reflection height was lowered by several kilometres, and the rate of electron density variation with height increased. Table 2 lists the four flares and the associated changes in ionospheric parameters. The electron density height profiles for all four flares, as well as the unperturbed profile, are shown in Figure 9. Not surprisingly, the stronger flares resulted in larger increases of D-region electron density. These results compare well to those of McRae and Thomson[13], who modelled a similar M-class flare where H' was found to decrease by ~8 km and β to increase by ~0.075 km^{-1}, as well as to the results presented in a larger study of stronger solar flares.[14]

Discussion

A waveguide propagation model was used to investigate the observed form of some of the UltraMSK signal perturbations. Our model was based on a flat, parallel plate waveguide formed between the Earth and the ionosphere, where the ionospheric aspect was determined by Wait's exponential profile whilst the lower boundary was characterised by appropriate conductivity and dielectric constant values. The reflection height of the wave in question and the refractive indices were determined, taking the effect of the ambient
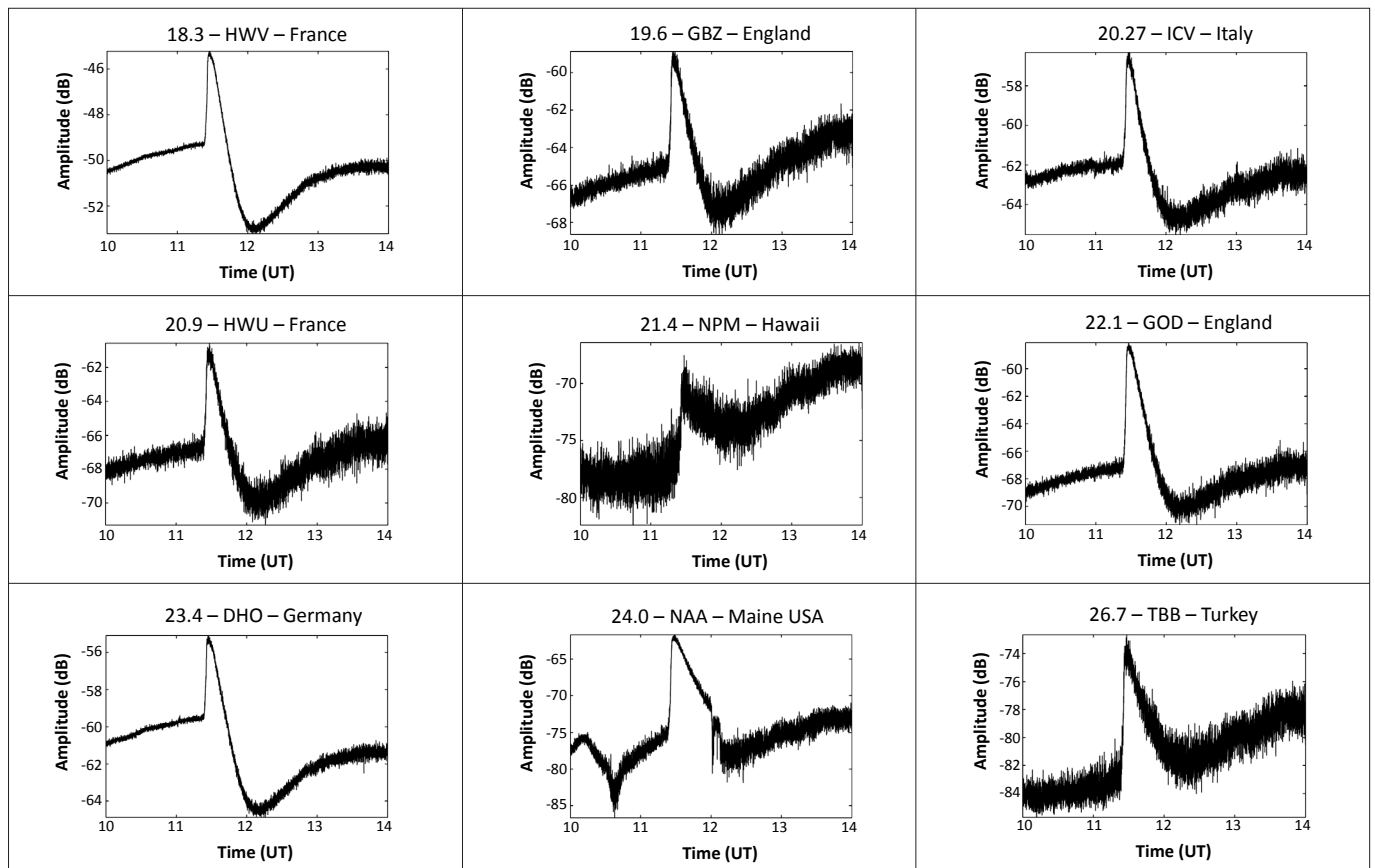
FIGURE 8: Power of nine signals monitored at SANAE IV. The solar flare at 11:27 UT on 12 February 2010 appears as a rapid increase, followed by a drop in the signal amplitudes.

TABLE 2: Date, duration and classification of four solar flares detected by SANAE IV, together with their change in ionospheric parameters – height (H') and exponential sharpness factor (β).

| Date	Start time	End time	Time of peak	Class	ΔH' (km)	Δβ (km⁻¹)
08 Feb 2010	11:00	11:18	11:14	C 1.8	2.2	0.016
08 Feb 2010	11:57	12:06	12:03	M 1.1	5.2	0.056
08 Feb 2010	13:32	13:50	13:47	M 2.0	6.5	0.086
12 Feb 2010	11:19	11:28	11:26	M 8.3	9.2	0.086
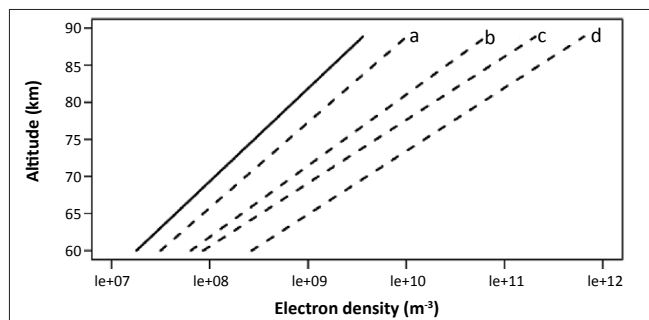
FIGURE 9: Unperturbed (solid line) and perturbed (a–d) electron density profiles during the solar flares that occurred on 08 February and 12 February 2010.

magnetic field into account. These values were then used to determine the modal angles that led to constructive interference of the reflections off the two boundaries. The electric fields for each mode were calculated as a function of propagation distance and the total field being the sum of all contributing modes. A solar flare effectively reduces the height of the ionosphere leading to a shift of the modal interference pattern towards the transmitter, as illustrated in Figure 10. For simplicity's sake, changes in H' but not β were investigated. The modelled temporal variation of H' is illustrated in Figure 11. The effects of a weak flare (ΔH' = −2 km) as well as a stronger flare (ΔH' = −6 km) for two hypothetical stations, A and B, located as shown in Figure 12, are plotted in Figures 13 and 14, respectively. The position of a station relative to the modal interference pattern, together with the strength of the flare, determines the response of the signal.

For a weak flare (ΔH' = −2 km), the interference pattern shifts (as shown in Figure 12) and then reverts to the unperturbed pattern again. For Station A, located approximately 500 km before a maximum, this means the receiver effectively rides up the slope towards the peak as the interference pattern is shifted towards the transmitter and back down as the height returns to the quiet-time value. This increase and then decrease is shown in the temporal response in Figure 13. An analogous response is observed for Station B, located approximately 400 km before a minimum, except that a decrease is experienced instead of an increase. For a larger flare (ΔH'= −6 km), the response can be slightly more complicated and the temporal profile of ionospheric height plays a major role (Figure 12). As a result of the very fast rise time of the perturbation, a large flare would result in the receiver 'skipping' over the maximum (A) or minimum (B) and this initial change in signal strength is not observed. Once the perturbation has reached its maximum value, it starts to decay slowly back to unperturbed conditions. The

receiver now spends a fair amount of time on the minimum or maximum it skipped during the rise and fully displays this change in signal strength shown in Figure 14.

The modelling results could be used to explain the initial increase and subsequent decrease in the measured amplitude for the M-class flare shown in Figure 6. Consider Receiver B in the modelling results for comparison with the real event (Figures 12 and 14). For a large flare, the ionosphere is ionised at such a great rate that the receiver does not resolve the initial decrease in signal as a result of the lowering of H' to between 74 km and 71 km (Figure 14, right panel). After the maximum perturbation in the ionosphere was reached at the time of peak flux (resulting in an increase of 4 dB in the signal amplitude), the ionosphere started to slowly recover and return to its initial condition. At this time, the ionosphere was fully experiencing the lowering of H' between 74 km and
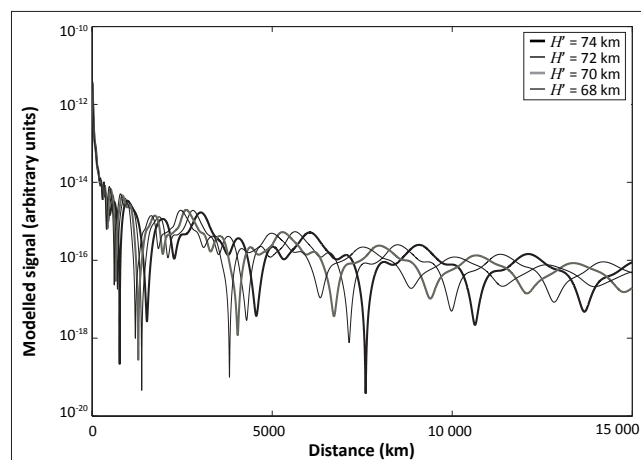

FIGURE 10: Modal interference pattern for different ionospheric heights (H'). As the reflection height of the ionosphere decreases, the modal interference pattern becomes more compressed, moving towards the transmitter.
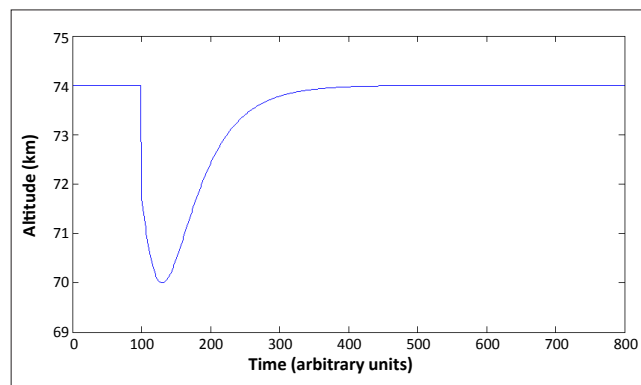
FIGURE 11: Modelled temporal variation in height showing the response of a typical solar flare, with a sharp rise and a slower decay.
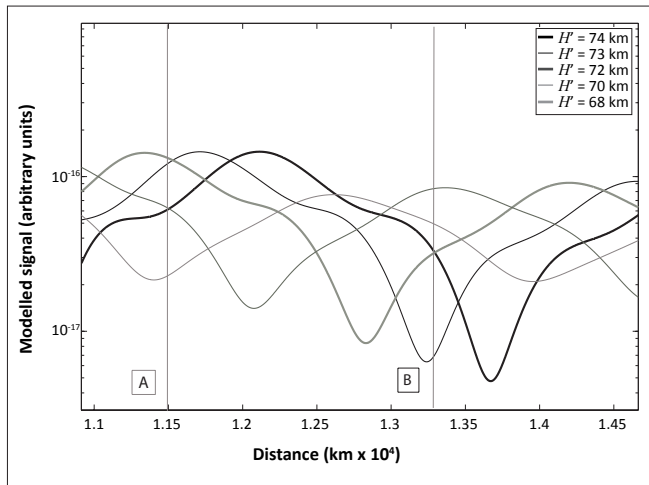
FIGURE 12: The interference pattern for different ionospheric heights (H'), as shown in Figure 10. The signal strength is dependent on the distance between the transmitter and the receiver. A and B mark the positions of two stations and the signal responses during a weak and a strong solar flare are shown in Figures 13 and 14, respectively.
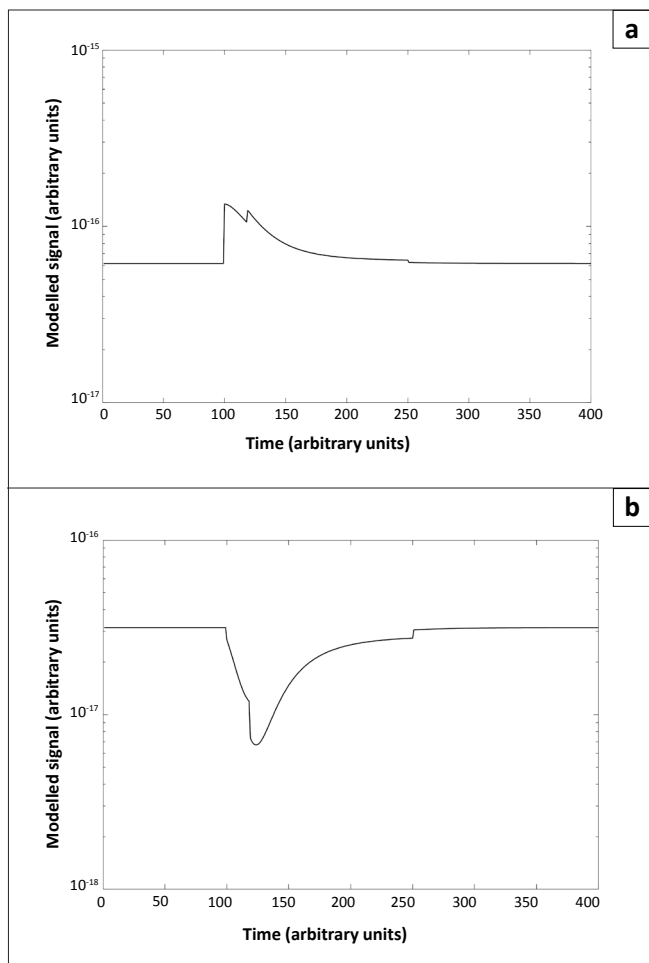
FIGURE 13: Temporal response of the signal at two stations: (a) Station A at 11 500 km and (b) Station B at 13 300 km, as a result of a weak flare. The ionospheric height is reduced by 2 km, causing the signal to change from the unperturbed thick black curve to the thin black curve in Figure 12.

71 km, leading to a decrease of 4 dB in the signal amplitude. The recovery phase of the ionosphere was much slower than the onset phase and led to a gradual change in H', reflecting a gradual return of the amplitude to unperturbed levels.
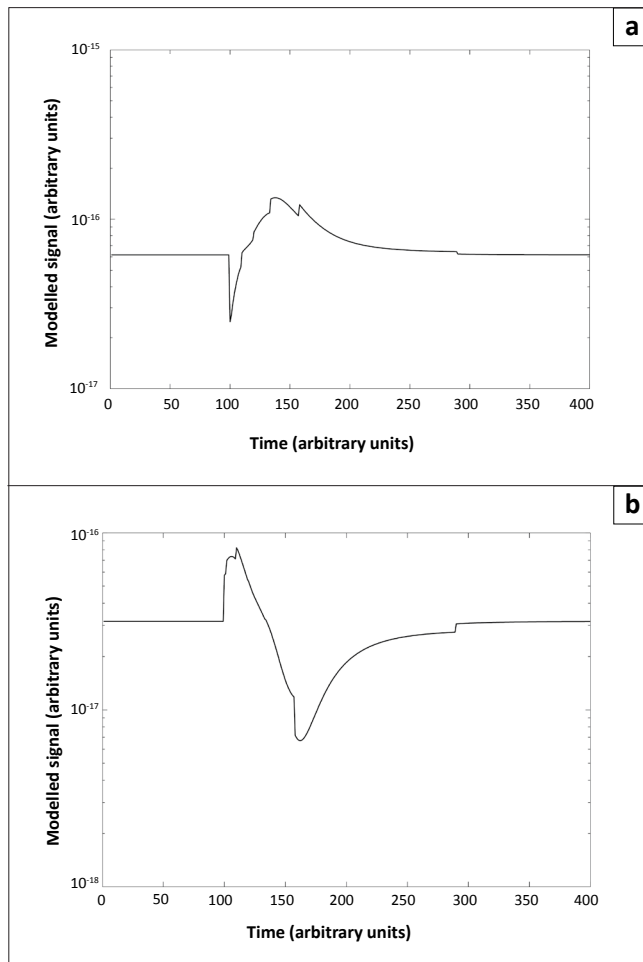
FIGURE 14: Temporal response of the signal at the two stations: (a) Station A at 11 500 km and (b) Station B at 13 300 km, as a result of a stronger flare The ionospheric height is reduced by 6 km, causing the signal to change from the unperturbed thick black curve to the thin grey curve in Figure 12.

Summary

The UltraMSK system described in this paper was previously installed on an omnidirectional whip antenna, but in February 2010 it was moved to a larger magnetic loop antenna, located at a greater distance from the SANAE IV base. This move improved the SNR significantly, which facilitates the analysis of weak signals whose amplitudes are close to the noise level of the system. The improvement is especially important during the day when the signal amplitude is depressed.

The functionality of the system was illustrated by the analysis of several M-class solar flares on 08 February and 12 February 2010. By using LWPC to model the ionospheric parameters at the time of the disturbances, it could be shown that the reflection height of the EIWG was lowered by between 2 km and 9 km during the flares, with the largest decrease occurring at the time of the strongest solar flare. The sharpness of the electron density gradient also increased, with a larger increase for the stronger events.

The form of the recorded signal could be investigated by comparing it with signals produced by a waveguide

propagation model. It was shown that the distance between the transmitting and receiving stations, as well as the temporal variation of ionospheric parameters, affects the shape of the signal as a result of shifts in the modal interference pattern, and such shifts can account for the decrease below the unperturbed values that followed some of the strong increases in the MSK signal amplitudes.

The results from the data and modelling are in accordance with typical ionospheric parameters during perturbed conditions and illustrate the system's capability in measuring ionospheric properties. With the new UltraMSK system, the signal was sufficiently elevated above the noise level compared to the previous system, mostly as a result of the larger antenna and moving the system away from the interfering infrastructure at the base. The presented data show that the UltraMSK system thus appears to be working in a satisfactory manner, and the data can be used to remotely probe the lower part of the ionosphere.

Acknowledgements

References

1. Thomson NR, Clilverd MA. Solar cycle changes in daytime VLF subionospheric attenuation. J Atmos Solar Terr Phys. 2000;62:601–608. doi:10.1016/S1364-6826(00)00026-2

2. Cummer SA, Inan US, Bell TF. Ionospheric D region remote sensing using VLF radio atmospherics. Radio Sci. 1998;33:1781–1792. doi:10.1029/98RS02381

3. Bickel JE, Ferguson JA, Stanley GV. Experimental observation of magnetic field effects on VLF propagation at night. Radio Sci. 1970;5:19–25. doi:10.1029/RS005i001p00019

4. Thomson NR. Experimental daytime VLF ionospheric parameters. J Atmos Terr Phys. 1993;55:173. doi:10.1016/0021-9169(93)90122-F

5. Collier AB, Hughes ARW. Digital VLF recording and analysis system for SANAE IV. S Afr J Sci. 2002;98(11/12):547–550.

6. Clilverd MA, Rodger CJ, Thomson NR, et al. Remote sensing space weather events: Antarctic–Arctic Radiation-belt (Dynamic) Deposition-VLF Atmospheric Research Konsortium network. Space Weather. 2009;7:15. doi:10.1029/2008SW000412

7. Dowden RL, Holzworth RH, Rodger CJ, et al. World-Wide Lightning Location Using VLF Propagation in the Earth–Ionosphere Waveguide. IEEE Antennas Propag Mag. 2008;50(5):40–60. doi:10.1109/MAP.2008.4674710

8. Barr R. A simple theoretical model of the diffraction of VLF electromagnetic waves by the Antarctic icecap. J Atmos Solar Terr Phys. 1992;54:1527–1533. doi:10.1016/0021-9169(92)90160-M

9. Wait JR. Electromagnetic waves in stratified media. Vol. 3 of International Series of Monographs on Electromagnetic Waves. New York: Pergamon Press; 1962.

10. Thomson NR. Experimental daytime VLF ionospheric parameters. J Atmos Terr Phys. 1993;55:173–184. doi:10.1016/0021-9169(93)90122-F

11. McRae WM, Thomson NR. VLF phase and amplitude: daytime ionospheric parameters. J Atmos Terr Phys. 2000;62:609–618. doi:10.1016/S1364-6826(00)00027-4

12. Deshpande SD, Subrahmanyam CV, Mitra AP. Ionospheric effects of solar flares – I. The statistical relationship between X-ray flares and SID's. J Atmos Terr Phys. 1972;34:211–227. doi:10.1016/0021-9169(72)90165-1

13. McRae WM, Thomson NR. Solar flare induced ionospheric D-region enhancements from VLF phase and amplitude observations. J Atmos Terr Phys. 2004;66:77–87. doi:10.1016/j.jastp.2003.09.009

14. Thomson NR, Rodger CJ, Clilverd MA. Large solar flares and their ionospheric D-region enhancements. J Geophys Res. 2005;110:6306–6316. doi:10.1029/2005JA011008